A multimodel study of the twentieth-century simulations of Sahel drought from the 1970s to 1990s

K. M. Lau,[1] S. S. P. Shen,[2] K.-M. Kim,[3] and H. Wang[4]

Received 5 July 2005; revised 7 December 2005; accepted 18 January 2006; published 15 April 2006.

[1] In this paper, we evaluate the performance of 19 coupled general circulation models (CGCMs) in twentieth-century simulations of the Sahel during the 1970s to 1990s. Correlation, regression, and cluster analyses are applied to observations and model outputs including Sahel monthly precipitation, evaporation, soil moisture, and sea surface temperature (SST). We find that only eight CGCMs (hit models) produce a reasonable Sahel drought signal, while seven CGCMs (miss models) produce excessive rainfall over the Sahel during the observed drought period. Even the model with the highest prediction skill of the Sahel drought could only predict the increasing trend of severe drought events but not the beginning and duration of the events. From analyses of the statistical characteristics of the hit and miss models, we conclude that a good simulation of the Sahel drought requires (1) a strong coupling between Sahel rainfall and Indian Ocean SST, with warm (cold) SST identified with Sahel drought (flood), (2) a significant coupling between Sahel rainfall and the Atlantic Ocean SST, with a warm equatorial Atlantic and cold extratropical North Atlantic coexisting with Sahel drought, and vice versa, and (3) a robust land surface feedback with strong sensitivity of precipitation and land evaporation to soil moisture. These three characteristics constitute sufficient conditions for a good simulation of Sahel drought in CGCMs.

Citation: Lau, K. M., S. S. P. Shen, K.-M. Kim, and H. Wang (2006), A multimodel study of the twentieth-century simulations of Sahel drought from the 1970s to 1990s, *J. Geophys. Res.*, *111*, D07111, doi:10.1029/2005JD006281.

1. Introduction

[2] Given prescribed observed sea surface temperature (SST) forcing, atmospheric general circulation models (GCMs) are known to have the ability to simulate and unravel the dynamical mechanisms of large-scale droughts, such as the 1930s droughts of the United States [*Schubert et al.*, 2004], the Sahel drought during the 1970–1980s [*Janicot et al.*, 1996; *Giannini et al.*, 2003], and the widespread drought in the United States, southern Europe, and Southwest Asia, during 1998–2002 [*Hoerling and Kumar*, 2003]. However, the ability of coupled GCMs (CGCMs) to simulate large-scale drought is largely unknown. Such ability is more difficult to evaluate, because it depends on, among other things, how well the SST is predicted and on how realistic is the coupling between SST and rainfall.

[3] The long-term drought over the Sahel region during 1970–1980s is one of the most pronounced signals of climate change with devastating impacts on society. The Sahel drought is known to be strongly influenced by sea surface temperature anomalies both globally and in regions adjacent to the African continent, as well as land-atmosphere feedback processes [*Folland et al.*, 1986; *Foutaine and Janicot*, 1996; *Hastenrath and Lamb*, 1977; *Lamb et al.*, 1986; *Rowell et al.*, 1995; *Ward*, 1992; *Xue and Shukla*, 1993]. As such, the Sahel drought provides an ideal test bed for evaluating the capability of CGCMs in simulating long-term drought, and the veracity of the model's representation of coupled atmosphere-ocean-land processes and their interactions. Previous studies have found that long-term Sahel drought may be induced from above-normal SST in the Indian Ocean and in the tropical Atlantic, and amplified by land-atmosphere interaction over the Sahel [*Folland et al.*, 1986; *Giannini et al.*, 2003]. On an interdecadal timescale, the Sahel rainfall is correlated with an interhemispheric SST dipole pattern, with negative SST anomalies in the North Atlantic and positive anomaly in the southern tropical Atlantic, including the Gulf of Guinea [*Hoerling et al.*, 2006; *Lamb*, 1978; *Rowell et al.*, 1995; *Zeng*, 2003]. On an interannual timescale, relationship between SST and Sahel rainfall is nonstationary, having a strong relationship to the Atlantic dipole before 1970, but weakens afterward. Since 1970, the correlation between SST anomalies in the eastern equatorial Pacific and Sahel rainfall, i.e., the impact of El Nino, appears to become more significant [*Janicot et al.*, 1996].

[4] In this paper, we explore the roles of SST coupling and land surface processes in producing the Sahel drought

[1]Laboratory for Atmospheres, NASA Goddard Space Flight Center, Greenbelt, Maryland, USA.
[2]Department of Mathematical and Statistical Sciences, University of Alberta, Edmonton, Alberta, Canada.
[3]Science Systems and Applications, Inc., Lanham, Maryland, USA.
[4]Goddard Earth Sciences and Technology Center, University of Maryland, Baltimore County, Baltimore, Maryland, USA.

Copyright 2006 by the American Geophysical Union.
0148-0227/06/2005JD006281$09.00

Table 1. List of the 19 Coupled Models and Their Relevant Information

Model	Model Acronym	Modeling Group(s)[a]	Country	Atmosphere Resolution	Ocean Resolution
1	CGCM3.1(T47)	CCCMA	Canada	3.75° × 3.71°	1.85° × 1.85°
2	CNRM-CM3	CNRM	France	2.81° × 2.79°	2° × 0.5°
3	CSIRO-Mk3.0	CSIRO	Australia	1.88° × 1.87°	1.88° × 0.84°
4	GFDL-CM2.0	GFDL	USA	2.5°× 2°	1° × 1/3°
5	GFDL-CM2.1	GFDL	USA	2.5° × 2°	1° × 1/3°
6	GISS-AOM	NASA/GISS	USA	4° × 3°	4° × 3°
7	GISS-EH	NASA/GISS	USA	5° × 4°	2° × 2°
8	GISS-ER	NASA/GISS	USA	5° × 4°	5° × 4°
9	FGOALS-g1.0	LASG/IAP	China	2.81° × 3.05°	1° × 1°
10	INM-CM3.0	INM	Russia	5° × 4°	2.5° × 2°
11	IPSL-CM4	IPSL	France	3.75° × 2.54°	2° × 1°
12	MIROC3.2(hires)	CCSR, NIES, FRCGC	Japan	1.13° × 1.12°	0.28° × 0.19°
13	MIROC3.2(medres)	CCSR, NIES, FRCGC	Japan	2.81° × 2.79°	1.4° × 0.5°
14	ECHAM5	MPI	Germany	1.88° × 1.87°	1.5° × 1.5°
15	CGCM2.3.2	MRI	Japan	2.81° × 2.79°	2.5° × 0.5°
16	CCSM3	NCAR	USA	1.41° × 1.40°	1.13° × 0.27°
17	PCM	NCAR	USA	2.81° × 2.79°	1.13° × 0.27°
18	UKMO-HadCM3	UKMO	UK	3.75° × 2.50°	1.25° × 1.25°
19	UKMO-HadGEM1	UKMO	UK	1.88° × 1.25°	1° × 1/3°

[a]CCCMA, Canadian Centre for Climate Modelling and Analysis; CNRM, Centre National de Recherches Météorologiques; CSIRO, Commonwealth Scientific and Industrial Research Organisation; GFDL, Geophysical Fluid Dynamics Laboratory; NASA/GISS, NASA Goddard Institute for Space Studies; LASG/IAP, National Key Laboratory of Numerical Modeling for Atmospheric Sciences and Geophysical Fluid Dynamics/Institute of Atmospheric Physics; INM, Institute of Numerical Mathematics; IPSL, Institut Pierre-Simon Laplace; CCSR, Center for Climate System Research; NIES, National Institute for Environmental Studies; FRCGC, Frontier Research Center for Global Change; MPI, Max Planck Institute; MRI, Mitsubishi Research Institute; NCAR, National Center for Atmospheric Research; UKMO, U.K. Met Office.

in CGCMs that participated in the twentieth-century coupled climate simulations of the Intergovernmental Panel for Climate Change Assessment Report 4 (IPCC AR4). Here, we focus on an interdecadal timescale with the objective of capturing the essence of model physics that are required to provide a good simulation of the Sahel drought. We will use simulation of the Standard Precipitation Index (SPI) over the Sahel region to rank and categorize the model, and to compare key model output parameters, i.e., rainfall, evaporation, soil moisture, and sea surface temperature (SST) to observations, according to the model categories. Cluster analysis is carried out to examine how well the simulated Sahel droughts are related to interactions of Sahel rainfall with SST of the Indian and the Atlantic oceans. We also examine the role of local land-atmosphere interaction from the covariability of Sahel rainfall, evaporation, and soil moisture for different CGCMs.

2. Data

[5] Our study is based on model outputs of 19 IPCC AR4 CGCMs [*Hegerl et al.*, 2003] and observations of global SST, Sahel precipitation, and the model-generated soil moisture. The monthly 0.5° × 0.5° precipitation data set (CRU TS2.0) is from the Climate Research Unit of the University of East Anglia is used [*Mitchell and Jones*, 2005]. The monthly 1° × 1° SST data are from the Hadley Centre. The data range from January 1871 to December 2000 [*Rayner et al.*, 2003]. No direct measurements of soil moisture are available for the global domain. For comparison with the model output, the Climate Prediction Center monthly global soil moisture data set [*Fan and van den Dool*, 2004] is used as "observed" soil moisture. The soil moisture product was generated by a one-layer bucket water balance model based on gauge observation of precipitation and the global surface temperature from the reanalysis data of the National Centers for Environmental Prediction and the National Center for Atmospheric Research. Since the bucket model is known to be unable to simulate realistic surface hydrology, the soil moisture used here should be treated as a reference product, and not as an observable. The IPCC AR4 CGCMs are driven by combination of realistic prescribed external forcing, including anthropogenic increase in greenhouse gases and sulfate aerosols, long-term variation in solar radiation, and volcanic eruptions. The models differ in both the magnitude of the external forcings and the way they are incorporated. The forcings have large uncertainties because of the limited observed data regarding magnitude, spatial pattern, and time evolution. Table 1 summarizes some basic information of the 19 coupled models. The models have different spatial and temporal resolutions, as well as different integration time periods covering the twentieth century. Our study is focused on the period 1950–1999 because of the reliability of the observed data and observed long-term Sahel droughts of the 1970–1990s. Since all the 19 models have reasonably high spatial resolution and have sufficient number of grid points in Sahel, a modeled climate parameter over Sahel is the simple average of the CGCM values at the grid points inside the Sahel domain, i.e., the latitude and longitude grid box (10°–20°N, 20°W to 40°E). No further spatial interpolation of the model output is needed. The July-August-September (JAS) observed precipitation accounts for 70% of the annual total over the Sahel. The signal of JAS precipitation change is quite pronounced in the time period of 1950–1999. Hence the JAS monthly mean precipitation is used in our investigation.

[6] For the land-atmosphere effect, a smaller subset of models is used because only 17 models provide total soil moisture data, and only 11 models provide surface soil

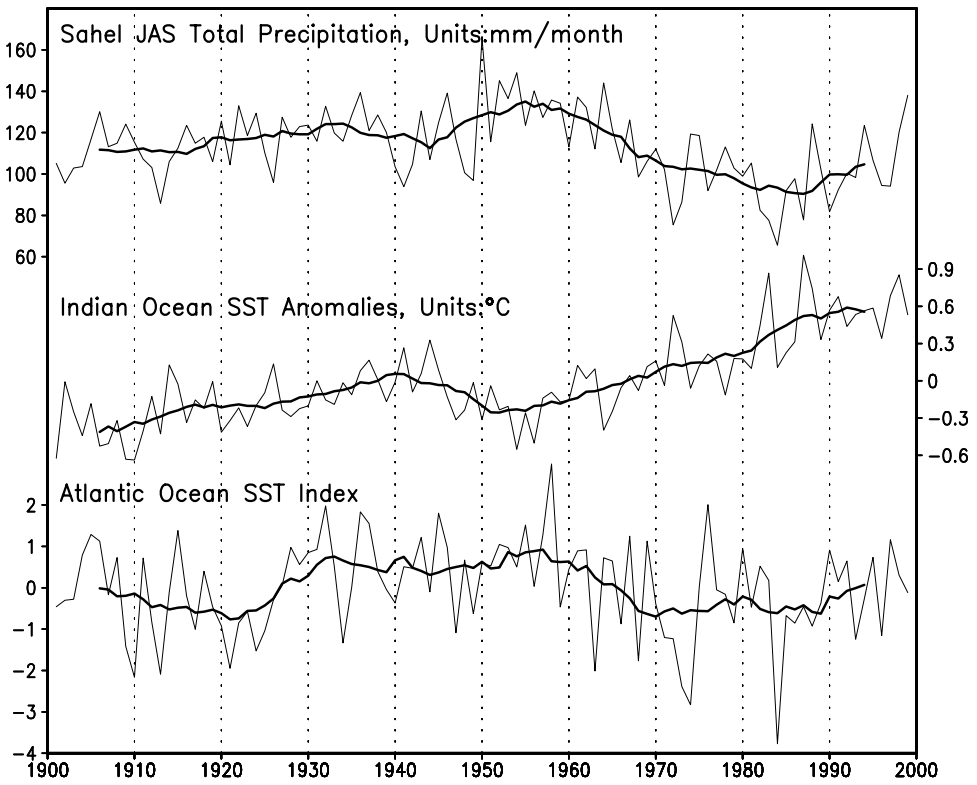

Figure 1. Time series of Sahel JAS precipitation, Indian Ocean SST, and the Atlantic Ocean SST index from 1950 to 1999.

moisture data. Given the model data availability, only the total soil moisture content is used.

3. Results

[7] The observed Sahel precipitation is defined as the spatially averaged monthly mean precipitation for JAS over the Sahel domain (10°–20°N, 20°W to 40°E) derived from the observed monthly CRU TS2.0 data (see Figure 1). The reconstructed HadISST [*Rayner et al.*, 2003] is used to generate the SST time series in Figure 1. The Indian Ocean SST is the area-averaged SST over the region (5°S to 5°N, 55°–75°E). Different domains are tested for the tropical Indian Ocean (5°S to 5°N, 55°–75°E), northern Indian Ocean (0°–20°N, 40°–100°E) and the whole Indian Ocean (20°S to 20°N, 40°–100°E). The tropical Indian Ocean SST appears to render the most clear out-of-phase signal with Sahel, and the results are insensitive to the domain chosen. This is most likely because the entire Indian Ocean SST is associated with a warming trend that encompasses the entire tropical oceans since the 1950s [*Lau and Weng*, 2001; *Giannini et al.*, 2003]. Similarly, the Atlantic SST dipole index is defined as the difference between the standardized SST over the North Atlantic (10°–40°N, 60°–20°W) and the standardized SST over the equatorial eastern Atlantic (10°S to 5°N, 30°W to 20°E) [*Zeng*, 2003]. A negative index value indicates a cooler North Atlantic Ocean and a warmer eastern tropical Atlantic Ocean, associated with a weakened western African monsoon and a southward shift of the Atlantic Intertropical Convergence Zone. Therefore the Atlantic SST dipole is positively correlated with Sahel precipitation.

[8] Figure 1 clearly shows the long-term inverse relationship between the observed Sahel precipitation and the observed Indian Ocean SST, as evident in the 11-year filtered data (smooth solid line in Figure 1). The relationship shows some degree of nonstationarity. The correlation of the filtered data for the entire period is −0.56, and increases to −0.88 during the latter half (1951–1994) of the period. The in-phase variation of the observed Sahel precipitation and the observed Atlantic SST index is also obvious in the figure. Here the correlation for the filtered data is 0.40 for the entire period, and 0.43 for the latter half For the purpose of comparing and evaluating the CGCMs, the correlations for 1951–1994 will be used.

[9] We use the SPI to quantify performance of the CGCMs' simulations of Sahel drought. SPI is a probabilistic type of drought monitoring index and is calculated via a nonlinear transformation that converts the precipitation data into a normally distributed, dimensionless random variable SPI [*McKee et al.*, 1993]. This transform explains that a drought over a region is manifested through the precipitation deficit relative to the region's precipitation history. On the basis of SPI, *McKee et al.* [1993] classified drought into four categories: mild ($-0.1 < SPI < 0$), moderate ($-1.5 < SPI < -1.0$), severe ($-2.0 < SPI < -1.5$), and extreme ($SPI < -2.0$). In the probability-based approach, the categories correspond to the probability of occurrence of 50.0%, 15.9%, 6.7%, and 2.4%, respectively.

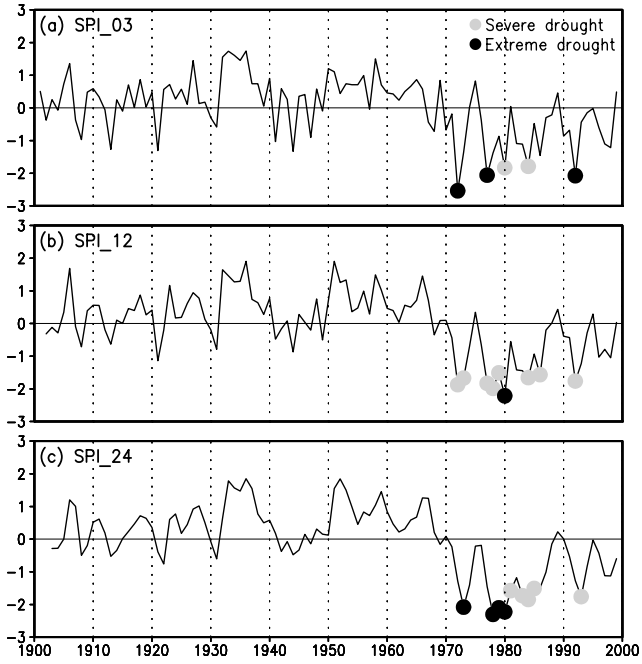

Figure 2. (a–c) Time series of observed SPI at the grid point (15°N, 13°W) in Sahel with different timescales. Years of severe and extreme drought are indicated by gray and dark circles, respectively.

[10] Since SPI allows multiple timescales, it can provide both an early warning of drought and an assessment of the drought severity. For example, the 24-month timescale SPI_24 at July of a given year is calculated on the basis of the mean precipitation of the 24 months at and before the July of that year. The SPI_24 at August and September can be calculated in the same way. The three month mean SPI_24 values of July, August, and September are used in our analysis. Thus each year has a JAS SPI_24 value. Figure 2 shows an example to demonstrates the utility of SPI time series in identifying droughts at different timescales at a single location (15°N, 13°W). Severe and extreme drought years are indicated by gray and black circles on the time series. The severe and extreme drought events from the 1970s to 1990s are shown at all the three timescales: 3, 12, and 24 months by large dark and gray large circles. Figure 2a shows five drought occurrences, and Figures 2b and 2c show nine for each. The increased number of occurrences from the late 1970s to the mid-1980s implies that no major precipitation events over Sahel from the late 1970s to mid-1980s can offset the long-term precipitation deficit. Because of the pronounced long-term drought over Sahel, SPI_24 is used in our subsequent analysis.

[11] Forty pairs of the SPI_24 values averaged over the Sahel region between observations and CGCM outputs from 1955 to 1994 are used to calculate the correlation coefficients (CC) displayed in Figure 3. The figure shows a bar chart of the CC sorted in ascending order. The eight solid black bars indicate CC greater than 0.26 (significant at the 5% level with 38 degrees of freedom) and reasonable agreement between observed and modeled values. Thus the models in this category are considered good simulations of the Sahel drought, i.e., a hit. The seven gray scale bars have CC less than −0.26 and indicate disagreement between the observed and modeled values, thus the models in this category are considered bad simulations of the Sahel drought, i.e., a miss. The other four grey scale bars have their CCs between −0.26 and 0.26 and are considered neutral. The two GFDL models (models 4 and 5) rank numbers one and two in the simulation of the Sahel drought according to our criterion.

[12] Since the Sahel's precipitation is negatively correlated with the Indian Ocean SST, if a model can simulate the Sahel precipitation correctly, most likely it should get this out-of-phase correlation with a correct sign. Figure 4a shows a scatter diagram of the CC between the modeled and observed precipitations with the CC between the modeled precipitation and Indian Ocean SST. All CC in this plot are calculated using 11-year moving averaged time series between 1955 and 1994, in order to focus on the long-term variations. P_{model} and P_{obs} shown in the figure are area-averaged simulated and observed precipitations, respectively. Indeed, all the eight hit models, indicated by the solid circles, are in the fourth quadrant, i.e., better

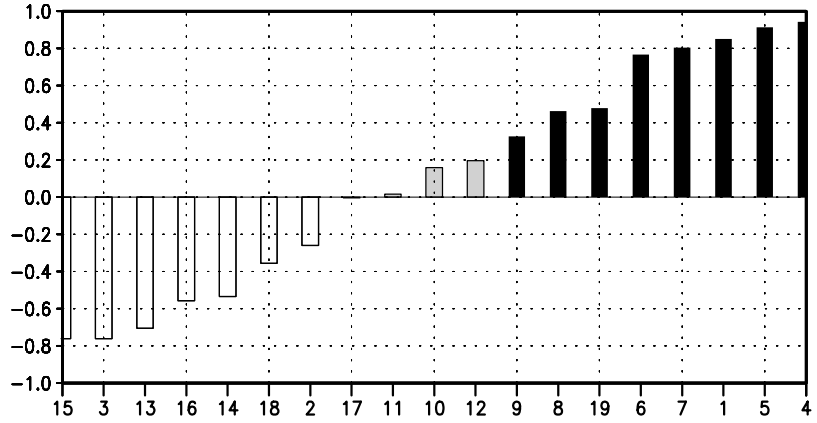

Figure 3. Correlation coefficients, marked on the vertical axis, between the SPI time series computed from observations and those from each model. The model numbers are sorted according to the correlation coefficients. Model numbers are shown on the horizontal axis.

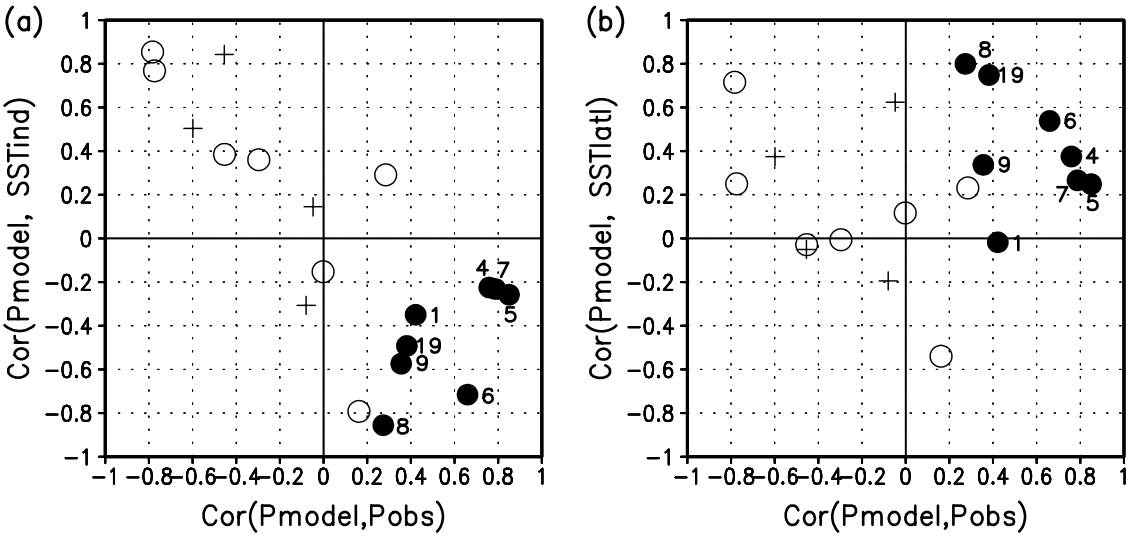

Figure 4. Scatter diagram of the correlation coefficients between the modeled and observed precipitations and the correlation coefficients between the modeled precipitation and (a) Indian Ocean SST and (b) Atlantic SST. Solid circles are for the best eight models (hits), open circles are for the worst seven models (misses), and the crosses indicate neutral models. Numbers next to the solid circles identify the eight hit models listed in Table 1.

simulation of Sahel drought requires better simulation of Indian Ocean coupling, as measured by the negative correlation between Sahel precipitation and Indian Ocean SST. Among the seven miss models indicated by open circles, five have positive correlations that are contrary to observation and two have negative correlations. These two models have correct phase between Indian Ocean SST and Sahel rainfall, but the simulation of Sahel drought is poor. The Indian Ocean SST has a warming trend for all models, but the coupling with Sahel rainfall varies greatly. The clustering of the model suggests that the ability of CGCM to simulate Sahel rainfall strongly depends on how well the model simulates the coupling between the Indian Ocean SST on the Sahel rainfall. This provides sufficient conditions for a long-term Sahel drought; that is, good Sahel drought simulation implies good coupling but not the other way round.

[13] Figure 4b shows a scatterplot of the CC between the modeled and observed precipitations with the CC between the modeled precipitation and Atlantic SST. All of the eight hit models, indicated by solid circles, are in the first quadrant with one on the margin. Among the seven miss models, two are in the second quadrant, and three are on the quadrant margin. The remaining two have the correct phase with respect to Atlantic SST, but the Sahel drought simulation is poor. The model clustering suggests that while most models simulate the correct sign of the coupling between Sahel rainfall and Atlantic SST dipole, this condition in itself is not a necessary condition for simulation of Sahel drought, i.e., good simulation of Atlantic SST and Sahel rainfall coupling does not necessarily imply good Sahel simulation.

[14] To understand the role of land-atmosphere coupling process in simulation of Sahel drought, the rate of change or sensitivity of land evaporation with respect to soil moisture is used as a proxy to represent the effect of feedback of land processes on the atmosphere. Figure 5a shows the cluster diagrams indicating the relationship between rainfall coupling with Indian Ocean SST and the sensitivity of evaporation to soil moisture. Regression slopes are used to measure the rate of change in model evaporation due to the change in total soil moisture. Because different models have different model soil depths, the regression slope is normalized with one standard deviation of soil moisture to facilitate comparison. The regression slope indicates how much moisture evaporates back to the atmosphere per unit change in soil moisture. The larger slope, the more sensitive is the evaporation to soil moisture, and more robust is the land feedback process. Figure 5a shows that overall the hit models (solid circles) have more robust land feedback processes compared to the miss models (open circles) and neutral models (crosses). The clustering of the models in the fourth quadrant, and on the right half of the second quadrant suggests that models that simulate the correct sign of the coupling between Indian Ocean SST and Sahel rainfall tend to have more robust land feedback processes.

[15] The CC between Sahel rainfall and soil moisture is used as a proxy to measure the degree in which the atmosphere forces the land. Large CC implies that the soil moisture quickly responds to rainfall. The ''observed'' correlation coefficient, depicted with a triangle in Figure 5b, between the Sahel precipitation and the tropical Indian Ocean SST is -0.89, and that between precipitation and the soil moisture is 0.93. All of the eight hit models are clustered close to the observation. Only one miss model (model 15, the MRI model) is in the same quadrant as the observed. Model 15, as indicated by the lone data point in the fourth quadrant in Figure 4b, fails to simulate the positive correlation between Sahel precipitation and the Atlantic Ocean SST index.

[16] Table 2 summarizes the correlation and regression results regarding the relative importance of SST coupling

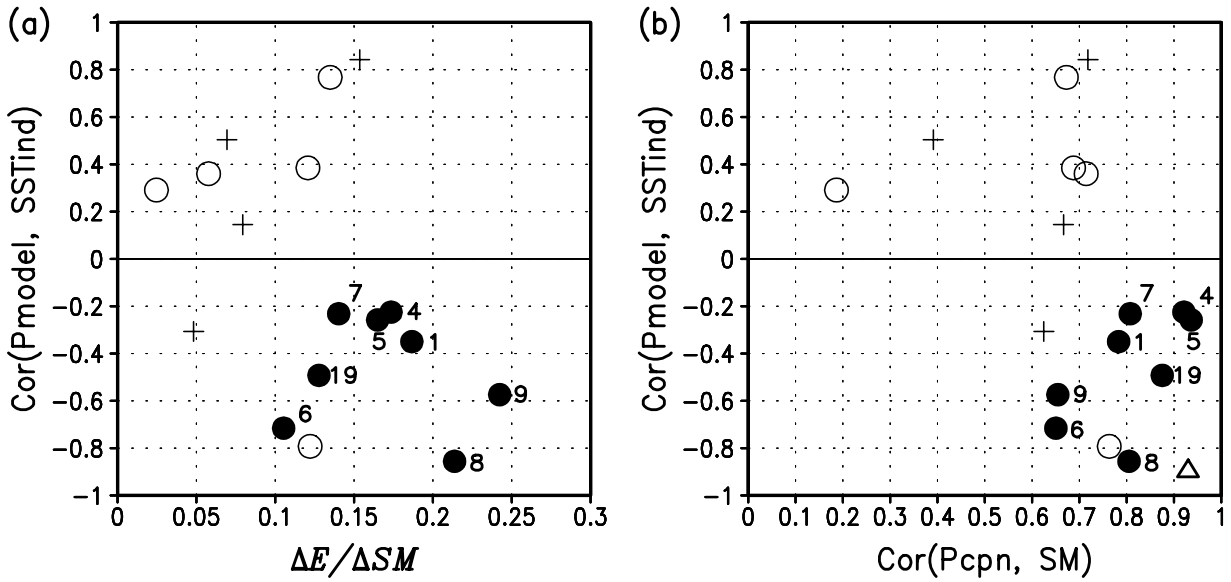

Figure 5. Scatter diagram between the correlation coefficients between the simulated Sahel precipitation and tropical Indian Ocean SST anomalies and (a) the rate of change of modeled evaporation as a function of the change in modeled soil moisture and (b) correlation coefficients between simulated Sahel precipitation and soil moisture. Solid circles identify the eight hit models, open circles are for the seven miss models, and the crosses indicate neutral models. The triangle in Figure 5b is determined by the values from observed precipitation and soil moisture. Numbers next to the solid circles indicate the eight hit models listed in Table 1.

and land-atmosphere interaction. The 19 coupled models are ranked in the same way as Figure 3 and shown in descending order in the first column. The second and fourth columns show the correlation between Sahel rainfall and Indian Ocean SST, and Atlantic Ocean SST dipole respectively. The ability of a model to simulate SST is evaluated with the CC between modeled and observed SST time series, which are shown in the third and fifth columns for the Indian Ocean and the Atlantic dipole respectively. As a measure of the sensitivity of rainfall and evaporation to soil moisture, the slopes of regression of soil moisture against precipitation and evaporation, normalized to standard deviation, are used and displayed in the sixth and seventh columns, respectively. Numbers in parentheses indicate the variance explained by the linear regression.

[17] Values larger than the median in each column are indicated in boldface, except the second column, where, because of the negative correlation, the values smaller than the median are in bold. All eight hit models show a negative correlation between Sahel precipitation and Indian Ocean SST as in the observation. Seven out of eight hit models show CC between observed and modeled Indian Ocean SSTs larger than the median value. This indicates the importance of Indian Ocean SST in simulating Sahel drought. The Atlantic SST dipole also plays a key role in long-term variation of Sahel precipitation as indicated by having six out of eight hit models showing high CC between Atlantic Ocean dipole and Sahel drought. Overall, Sahel precipitation from hit models shows good relations with both Indian Ocean SST and Atlantic Ocean SST index. No miss models or neutral models have good correlations between rainfall and SST in both oceans. For example, model 15 (the MRI CGCM2.3.2) is the worst according to our criteria and yet the CC between Sahel precipitation and Indian Ocean SST is the second best (-0.79). This may be the result of poor simulation of the coupling between Sahel precipitation and Atlantic Ocean SST (large negative correlation, -0.51, and with the wrong sign compared to observation). The bottom ranking of this model may also be contributed in part by its relatively weak atmosphere-land coupling as shown in columns 4 and 5 (see discussion in next paragraph). Interestingly, the CCs between modeled and observed Indian Ocean SST (the third column) and CCs between modeled and observed Atlantic Ocean SST index (the fifth column) did not show consistent results as in relationships between SST and Sahel precipitation. This indicates that a good simulation of Indian Ocean SST and Atlantic Ocean SST dipole does not guarantee a good simulation of Sahel precipitation. For better simulation of Sahel rainfall, the model has to be able to simulate the coupling between SSTs and Sahel precipitation.

[18] As stated before, good SST-rainfall coupling is not the only factor conducive to a good Sahel drought simulations. Land-atmosphere feedback also plays an important role [e.g., *Zeng et al.*, 1999]. To wit, model 4 (the GFDL-CM2.0), the top ranked model has only moderate rain-SST coupling with the Indian and the Atlantic Ocean, but has the strongest regression slope of precipitation to soil moisture (column 6), and strong sensitivity of evaporation to soil moisture (last column). Overall, six out of eight hit models show regression slopes between precipitation and soil moisture larger than the median. Given the fact that precipitation is the major input to soil moisture, a large regression slope of precipitation to soil moisture can also mean that more rainfall is required to produce a unit change in soil moisture in hit models, suggesting rainfall does not increase

Table 2. Correlation Coefficients and Regression Slopes That Relate Sahel Precipitation to Indian Ocean SST, Atlantic Ocean SST, Sahel Evaporation, and Sahel Soil Moisture

Model	$\gamma_{P_{Sahel}T_{Ind}}$	$\gamma_{T_{model\_Ind}T_{obs\_Ind}}$	$\gamma_{P_{Sahel}T_{Atl}}$	$\gamma_{T_{model\_Atl}T_{obs\_Atl}}$	$b_{P,SM}(r^2)$	$b_{E,SM}(r^2)$
			Hit Models			
4	−0.22	0.15	**0.38**	**0.54**	**0.761** (0.85)	**0.174** (0.76)
5	**−0.26**	0.18	0.25	0.17	**0.682** (0.88)	**0.165** (0.80)
1	**−0.35**	**0.58**	−0.02	**0.71**	0.298 (0.61)	**0.187** (0.60)
7	**−0.23**	0.22	**0.27**	0.03	**0.343** (0.65)	**0.140** (0.66)
6	**−0.72**	0.22	**0.54**	**0.75**	0.143 (0.42)	0.105 (0.53)
19	**−0.49**	0.09	**0.75**	**0.33**	**0.314** (0.77)	**0.128** (0.78)
8	**−0.86**	**0.23**	**0.80**	0.18	**0.332** (0.65)	**0.214** (0.76)
9	**−0.57**	**0.32**	**0.34**	−0.68	**0.322** (0.43)	**0.242** (0.46)
			Neutral Models			
12	0.15	**0.25**	**0.62**	**0.48**	**0.347** (0.44)	0.079 (0.62)
10	0.50	0.19	**0.37**	**0.25**	0.071 (0.15)	0.069 (0.23)
11	**−0.31**	**0.35**	−0.19	**0.35**	0.046 (0.39)	0.048 (0.49)
17	0.84	0.19	−0.05	−0.30	0.286 (0.52)	**0.154** (0.61)
			Miss Models			
2	−0.15	**0.44**	0.12	−0.46		
18	0.77	**0.25**	0.25	−0.59	**0.319** (0.45)	**0.135** (0.59)
14	0.36	0.11	−0.01	−0.01	0.175 (0.51)	0.058 (0.46)
16	0.29	0.10	0.23	**0.48**	0.046 (0.03)	0.025 (0.05)
13	0.39	**0.24**	−0.03	**0.35**	**0.555** (0.47)	0.121 (0.63)
3	0.85	0.22	**0.72**	−0.73		
15	**−0.79**	**0.28**	−0.54	−0.32	0.198 (0.58)	0.122 (0.58)

soil moisture immediately in hit models. Instead, other processes, including runoff and evaporation back to atmosphere, play equally important roles in land-atmosphere feedback process. Indeed, seven hit models show larger than median regression slope between evaporation and soil moisture. Six out of these models also show strong sensitivity of evaporation to soil moisture. With few exceptions, all neutral and miss models show a lack of sensitivity of rainfall and/or evaporation to soil moisture. Model 18 (the UKMO model) shows that strong land feedback process in itself cannot lead to good simulation of Sahel drought, if the SST coupling is weak or of the wrong sign.

[19] To further evaluate CGCM simulations of the Sahel drought, we examine the models' capability to produce severe drought (probability of occurrence 6.7%) and extreme drought (probability of occurrence 2.3%) on the basis of SPI_24. The areas affected by severe and extreme drought from hit and miss models are compared to observation. Figures 6a and 6b show the percent coverage of the severe-to-extreme events, and extreme events only over the Sahel (10°–20°N, 20°W to 40°E). Following *McKee et al.* [1993], severe and extreme droughts occur when the SPI_24 is less than −1.5 and −2.0, respectively. The observed severe and extreme drought area (solid line) calculated on the basis of SPI_24 using CRU TS2.0 monthly precipitation shows rather complex long-term variations. Observation (thick solid lines in Figures 6a and 6b) shows that there is an increasing trend in severe-and-extreme droughts since the 1970 with almost no drought between the 1950 and 1970s, maximum drought occurrence in the mid-1970 and mid-1980s, and a recovery toward the pre-1950 level since the mid-1990s. Prior to the 1970s, the hit and miss models (indicated by crosses in Figures 6a and 6b) do not show any significant differences, but the difference becomes obvious after the 1970s. For severe-and-extreme droughts (Figure 6a), hit models correctly produce an increasing trend of severe and extreme drought events during the last three decades, but not the miss models. Individual hit models can produce droughts as strong as the observed, while the model ensemble mean (shown by the thin solid line with area under the curve shaded) is much smaller than the observed during the 1970–1990s. Interestingly, the ensemble mean of hit models simulate quite well the reduced magnitude of the pre-1950 droughts. As expected, even the hit models cannot correctly simulate the magnitude and duration of individual drought events. Needless to say, the miss models show no preferred drought during observed Sahel drought period. For extreme drought events, observation shows a peak in the mid-1970s and in mid-1980s. The hit models show a tendency for increase extreme drought in about the same period (Figure 6c), but little skill in simulating the beginning and ending of such events. Miss models clearly have zero skill in reproducing the extreme drought events.

[20] It is intriguing, as seen from Figure 6a, that the hit models appear to have correct time markers that separate the 1970s–1990s from the earlier period. The CGCMs are coupled systems with external forcings, including solar forcing, greenhouse gases, aerosols, and volcanic eruption, that are quantified as an energy input to the systems. Oscillations and nonlinear trends of solar radiation and greenhouse gases do not have a clear distinction before and after the 1970s. In all the external forcings, only volcanic eruption has a specific time marker. Stratospheric aerosol experienced a sudden increase around the 1960s because of the relatively quiet volcanic activities before, and the unusually active eruptions after, the 1960s. Figure 6 shows that the eight hit models respond well to the aerosol time mark and correctly simulate not only the increasing trend of Sahel drought but also the area affected by extreme drought events. It may be speculated that the increasing

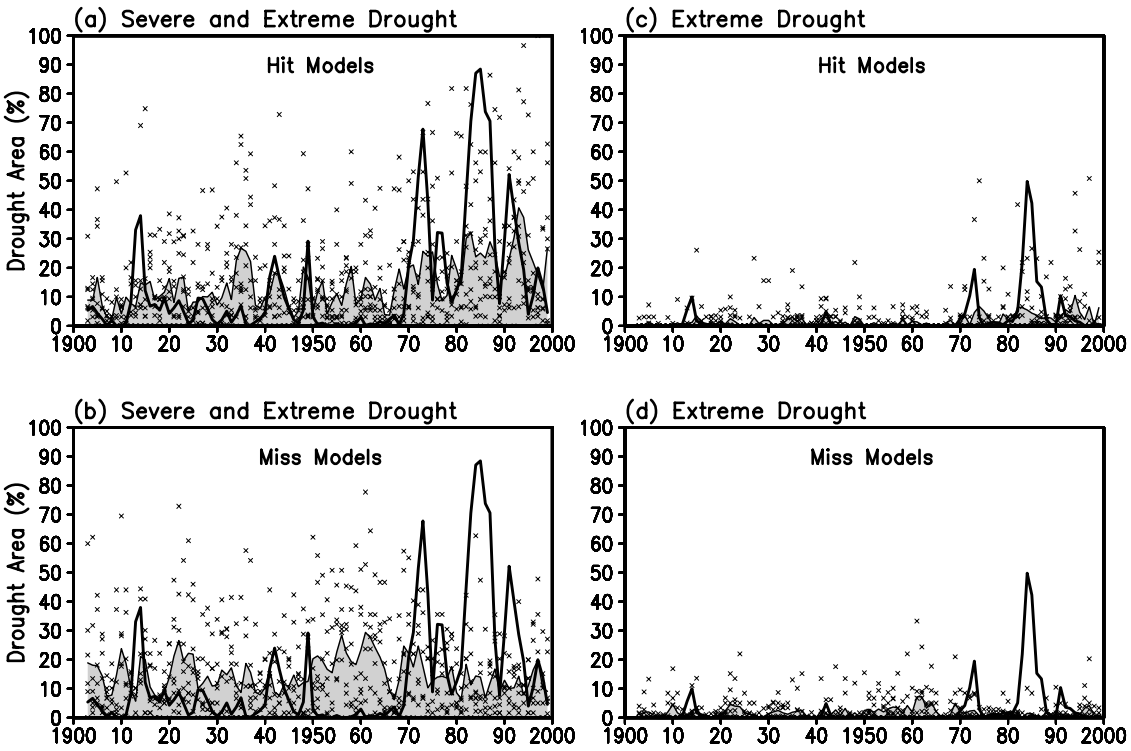

Figure 6. Time series of the percentage area of severe and/or extreme drought over the Sahel (10°–20°N, 20°W to 40°E). The thick solid line is that computed from observed precipitation data. The crosses are from (a) eight hit models and (b) seven miss models. (c and d) Same as Figures 6a and 6b but for extreme drought events. The model ensemble mean is shown by the thin solid line with light shaded area.

tropospheric and stratospheric aerosols cools the northern Atlantic Ocean and provides favorable conditions (i.e., the negative Atlantic Ocean SST index) for the Sahel drought. This is consistent with recent results which show that a reduction of surface radiation by indirect effects of anthropogenic sulfate aerosols may cause cooling of the North Atlantic and warming of the South Atlantic, and contribute to a prolonged Sahel drought [*Rotstayn and Lohmann*, 2002].

4. Conclusion and Discussion

[21] We have evaluated the capability of 19 CGCMs in simulating the Sahel drought in 100-year simulations of the twentieth-century climate with realistic external forcings. The models are evaluated according to correlation between Sahel rain and sea surface temperature in the Indian Ocean and the Atlantic Ocean, and covariability of rainfall, evaporation and soil moisture over the Sahel region. We find that only eight models (the hit models) produce a reasonable Sahel drought signal, seven models (the miss models) produce excessive rainfall over Sahel during the observed drought period, and four models (the neutral models) show no significant deviation from normal. Even the model with the highest simulation skill for the Sahel drought could only simulate the increasing trend of severe drought events but not the magnitude, nor the beginning time and duration of the events. From analysis of the characteristics of hit and miss models, we find a good simulation of Sahel drought in coupled models requires (1) a strong coupling between Sahel rainfall and Indian Ocean SST with warm (cold) SST identified with Sahel drought (flood), (2) a significant coupling between Sahel rainfall and the Atlantic SST dipole index, with colder North Atlantic and warmer tropical eastern Atlantic identified with Sahel drought and vice versa, and (3) a robust land feedback process with strong sensitivity of precipitation and evaporation to soil moisture over the Sahel. These constitute a set of strongly sufficient, but only weakly necessary conditions for good Sahel drought simulation by CGCMs; that is, all hit models have at least two of the above conditions satisfied, and models that satisfy all three conditions form a subset of hit models, but none show up as miss or neutral models.

[22] Previous results have shown that the warming of the Indian Ocean in recent decades may be part of a global warming pattern on interdecadal or longer timescales (*Lau and Weng* [2001] and others). Thus the coupling of the Indian Ocean SST to Sahel drought, may be identified with the warming of the global tropical oceans [*Giannini et al.*, 2003]. We also found that a good simulation of the Indian Ocean SST and/or Atlantic Ocean SST in itself is not a sufficient condition for Sahel drought. A strong coupling between SST and Sahel rainfall, and robust land surface feedback processes are crucial. Physically, the mechanism may work as follows: The warmer water in the Indian Ocean and the eastern Atlantic enhances deep convection over the ocean and weakens the continental convergence and hence reduces monsoon moisture and rainfall over land. Reduced rainfall leads to less soil moisture and depending on the strength of the land surface feedback, there will be

less evaporation over land, further reducing atmospheric moisture and exacerbating the drought. Examination of individual models (not shown) appears to broadly bear out the above scenario.

[23] Although the out-of-phase increase of the Indian Ocean SST and the in-phase decrease of the Atlantic SST index are two key controls for a long-term Sahel drought simulation in CGCMs, the notion of SST-driven Sahel drought still has room for debate since they constitute only sufficient but only weakly necessary conditions. Any climate forcings that alter land surface feedback processes including aerosols, land use and land change, and interactive vegetation may play a role in amplifying the SST induced responses. Our present results only provide check points for model evaluation for future research on these important topics.

[24] **Acknowledgments.** We acknowledge the international modeling groups for providing their data for analysis, the Program for Climate Model Diagnosis and Intercomparison (PCMDI) for collecting and archiving the model data, the JSC/CLIVAR Working Group on Coupled Modeling (WGCM) and their Coupled Model Intercomparison Project (CMIP) and Climate Simulation Panel for organizing the model data analysis activity, and the IPCC WG1 TSU for technical support. The IPCC Data Archive at Lawrence Livermore National Laboratory is supported by the Office of Science, U.S. Department of Energy. This study was supported in part by U.S. CLIVAR Climate Model Evaluation Project (CMEP) and the Modeling, Analysis, and Prediction (MAP) Program of NASA. The SST and precipitation data were obtained from the UCAR Scientific Computing Division (SCD) Data Supporting Section after a license was obtained from the CRU and Hadley Centre. S. S. P. Shen thanks the Goddard Earth Sciences and Technology Center for hosting his visit while this work was performed.

References

Fan, Y., and H. van den Dool (2004), Climate Prediction Center global monthly soil moisture data set at 0.5° resolution for 1948 to present, *J. Geophys. Res.*, *109*, D10102, doi:10.1029/2003JD004345.

Folland, C. K., T. N. Palmer, and D. E. Parker (1986), Sahel rainfall and world wide sea temperatures, 1901–85, *Nature*, *320*, 602–607.

Foutaine, B., and S. Janicot (1996), Sea surface temperature fields associated with West African rainfall anomaly types, *J. Clim.*, *9*, 2935–2940.

Giannini, A., R. Saravanan, and P. Chang (2003), Oceanic forcing of Sahel rainfall on interannual to interdecadal time scales, *Science*, *302*, 1027–1030.

Hastenrath, S., and P. Lamb (1977), Some aspects of circulation and climate over the eastern equatorial Atlantic, *Mon. Weather Rev.*, *105*, 1019–1023.

Hegerl, G., G. Meehl, C. Covey, M. Latif, B. McAveney, and R. Stouffer (2003), 20C3M: CMIP collecting data from 20th century coupled model simulations, *CLIVAR Exch. 26,* pp. S3–S5, Int. CLIVAR Proj. Off., Southampton, UK.

Hoerling, M., and A. Kumar (2003), The perfect ocean for drought, *Science*, *299*, 691–694.

Hoerling, M. P., J. W. Hurrell, and A. Philips (2006), Detection and attribution of twentieth-century northern and southern African rainfall change, *J. Clim.*, in press.

Janicot, S., V. Moron, and B. Fontaine (1996), Sahel drought and ENSO dynamics, *Geophys. Res. Lett.*, *23*, 515–518.

Lamb, P. J. (1978), Large-scale tropical Atlantic surface circulation patterns associated with sub-Saharan weather anomalies, *Tellus*, *30*, 240–251.

Lamb, P. J., R. A. Peppler, and S. Hastenrath (1986), Interannual variability in the tropical Atlantic, *Nature*, *322*, 238–240.

Lau, K. M., and H. Weng (2001), Decadal-interdecadal and global warming signals in sea surface temperature during 1955–97, *J. Clim.*, *12*, 1257–1267.

McKee, T. B., N. J. Doesken, and J. Kleist (1993), The relationship of drought frequency and duration to time scales, paper presented at 8th Conference on Applied Climatology, Am. Meteorol. Soc., Anaheim, Calif., 17–22 Jan.

Mitchell, T. D., and P. D. Jones (2005), An improved method of constructing a database of monthly climate observations and associated high-resolution grids, *Int. J. Climatol.*, *25*, 693–712.

Rayner, N. A., D. E. Parker, E. B. Horton, C. K. Folland, L. V. Alexander, D. P. Rowell, E. C. Kent, and A. Kaplan (2003), Global analyses of sea surface temperature, sea ice, and night marine air temperature since the late nineteenth century, *J. Geophys. Res.*, *108*(D14), 4407, doi:10.1029/2002JD002670.

Rotstayn, L. D., and U. Lohmann (2002), Tropical rainfall trends and indirect aerosol effect, *J. Clim.*, *15*, 2103–2116.

Rowell, D. P., C. K. Folland, K. Maskell, and M. N. Ward (1995), Variability of summer rainfall over tropical North Africa (1906–92): Observation and modeling, *Q. J. R. Meteorol. Soc.*, *121*, 669–704.

Schubert, S. D., M. J. Suarez, P. J. Pegion, R. D. Koster, and J. T. Bacmeister (2004), On the cause of the 1930s dust bowl, *Science*, *303*, 1855–1859.

Ward, N. (1992), Provisionally corrected surface wind data, worldwide ocean-atmosphere surface fields and Sahel rainfall variability, *J. Clim.*, *5*, 454–475.

Xue, Y., and J. Shukla (1993), The influence of land surface properties on Sahel climate: Part Desertification, *I., J. Clim.*, *6*, 2232–2245.

Zeng, N. (2003), Drought in the Sahel, *Science*, *302*, 999–1000.

Zeng, N., J. D. Neelin, K.-M. Lau, and C. J. Tucker (1999), Enhancement of interdecadal climate variability in the Sahel by vegetation interaction, *Science*, *286*, 1537–1540.

K.-M. Kim, Climate and Radiation Branch, NASA Goddard Space Flight Center, Code 613.2, Greenbelt, MD 20771, USA.

K. M. Lau, Laboratory for Atmospheres, NASA Goddard Space Flight Center, Greenbelt, MD 20771, USA. (lau@climate.gsfc.nasa.gov)

S. S. P. Shen, Department of Mathematical and Statistical Sciences, University of Alberta, Edmonton, AB, Canada T6G 2G1.

H. Wang, Goddard Earth Sciences and Technology Center, University of Maryland, Baltimore County, Baltimore, MD 21228, USA.